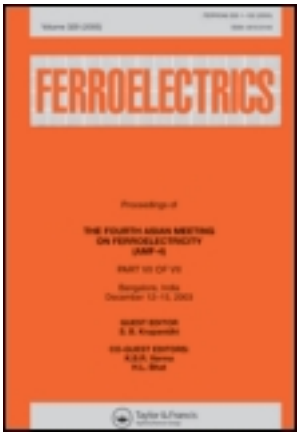

Ferroelectrics
Publication details, including instructions for authors and subscription information:
http://www.tandfonline.com/loi/gfer20

Optical Properties and Electronic Band Structure of Topological Insulators (on $A^5{}_2B^6{}_3$ Compound Based)

H. Koc [a], Amirullah M. Mamedov [b] & Ekmel Ozbay [b]
[a] Department of Physics, Siirt University, 56100, Siirt, Turkey
[b] Nanotechnology Research Center (NANOTAM), Bilkent University, 06800, Bilkent, Ankara, Turkey
Published online: 20 Sep 2013.

To cite this article: H. Koc, Amirullah M. Mamedov & Ekmel Ozbay (2013) Optical Properties and Electronic Band Structure of Topological Insulators (on $A^5{}_2B^6{}_3$ Compound Based), Ferroelectrics, 448:1, 29-41, DOI: 10.1080/00150193.2013.822277

To link to this article: http://dx.doi.org/10.1080/00150193.2013.822277

Ferroelectrics, 448:29–41, 2013

ISSN: 0015-0193 print / 1563-5112 online
DOI: 10.1080/00150193.2013.822277

Taylor & Francis
Taylor & Francis Group

Optical Properties and Electronic Band Structure of Topological Insulators (on $A_2^5B_3^6$ Compound Based)

H. KOC,[1,*] AMIRULLAH M. MAMEDOV,[2]
AND EKMEL OZBAY[2]

[1]Department of Physics, Siirt University, 56100 Siirt, Turkey
[2]Nanotechnology Research Center (NANOTAM), Bilkent University, 06800 Bilkent, Ankara, Turkey

We have performed a first principles study of structural, electronic, and optical properties of rhombohedral Sb_2Te_3 and Bi_2Te_3 compounds using the density functional theory within the local density approximation. The lattice parameters, bulk modulus, and its pressure derivatives of these compounds have been obtained. The linear photon-energy dependent dielectric functions and some optical properties such as the energy-loss function, the effective number of valance electrons and the effective optical dielectric constant are calculated and presented in the study.

Keywords: Ab initio calculation; electronic structure; optical properties

1. Introduction

Sb_2Te_3 and Bi_2Te_3, the members of compounds with the general formula $A_2^V B_3^{VI}$ ($A =$ Bi, Sb and $B =$ S, Se, Te), are narrow-band gap semiconductors with rhombohedral layered crystal structure. Sb_2Te_3 and Bi_2Te_3 are well-known topological insulators [1–7], extraordinary thermoelectric materials at ambient temperature [8] and the possible topological superconductors [9] with surface states consisting of a single Dirac cone at the Γ. All of these have made $A_2^V B_3^{VI}$ compounds as the subject of intensive investigation both in fundamental and applied research. These compounds possess the rhombohedral crystal structure with five atoms per unit cell belonging to the space group $D_{3d}^5(R\bar{3}\,m)$. Sb_2Te_3 and Bi_2Te_3 can be used for many different applications such as power generation and cooling devices [10]. Thermoelectric power generators and cooler have many advantages over conventional refrigerators and power generators such as long life, no moving parts, no green house gases, no noise, low maintenance and high reliability [11–13].

In the past, some detailed works [6, 7, 14, 15] have been carried out on the structural and electronic properties of these compounds. Zhang et al. [6] study in detail the topological nature and the surface states of this family of compounds using the fully self-consistent ab initio calculations in the framework of density functional theory. Zhang et al. [7] focused on layered, stoichiometric crystals Sb_2Te_3, Sb_2Se_3, Bi_2Te_3 and Bi_2Se_3 using ab initio calculations in the framework of the Perdew-Burke-Ernzerhof type generalized gradient

Received September 25, 2012; in final form March 8, 2013.
*Corresponding author. E-mail: husnu_01_12@hotmail.com

approximation of the density functional theory. Wang et al. [14] calculated the electronic structures of Sb_2Te_3 and Bi_2Te_3 crystals using the first-principles full potential linearized augmented plane-wave method. Yavorsky et al. [15] performed calculations of the electronic structures of Sb_2Te_3 and Bi_2Te_3 compounds by means of the screened Korringa-Kohn-Rostoker (KKR) Green's function method in the atomic sphere approximation (ASA) within local density approximation of the density functional theory. Choi et al. [16] reported the crystal growth and ferromagnetic (FM) properties of Mn-doped Sb_2Te_3 and Bi_2Te_3 bulk crystals.

As far as we know, no ab initio general potential calculations of the density of state, charge density and the optical properties of the Sb_2Te_3 and Bi_2Te_3 have been reported in detail. In the present work, we have investigated the structural, electronic, and photon energy-dependent optical properties of the Sb_2Te_3 and Bi_2Te_3 crystals. The method of calculation is given in Section 2; the results are discussed in Section 3. Finally, the summary and conclusion are given in Section 4.

2. Method of Calculation

Our calculations have been performed using the density functional formalism and local density approximation (LDA) [17] through the Ceperley and Alder functional [18] as parameterized by Perdew and Zunger [19] for the exchange-correlation energy in the SIESTA code [20, 21]. This code calculates the total energies and atomic forces using a linear combination of atomic orbitals as the basis set. The basis set is based on the finite range pseudoatomic orbitals (PAOs) of the Sankey-Niklewsky type [22], generalized to include multiple-zeta decays.

The interactions between electrons and core ions are simulated with separable Troullier-Martins [23] norm-conserving pseudopotentials. We have generated atomic pseudopotentials separately for atoms, Sb, Bi and Te by using the $5s^25p^3$, $6s^26p^3$ and $5s^25p^4$ configurations, respectively. The cut-off radii for present atomic pseudopotentials are taken as s: 3.82 au, p: 2.71 au, 2.92 au for the d and f channels of Bi, s:3.62 au, p:2.40 au, 2.78 au for the d and f channels of Te and 2.35 for the s, p, d and f channels of Sb.

Siesta calculates the self-consistent potential on a grid in real space. The fineness of this grid is determined in terms of an energy cut-off E_c in analogy to the energy cut-off when the basis set involves plane waves. Here by using a double-zeta plus polarization (DZP) orbitals basis and the cut-off energies between 100 and 500 Ry with various basis sets, we found an optimal value of around $425Ry$ for Sb_2Te_3 and Bi_2Te_3. For the final computations, 54 k-points for Sb_2Te_3 and Bi_2Te_3 were enough to obtain the converged total energies ΔE to about 1meV/atoms.

3. Results and Discussion

3.1 Structural Properties

All physical properties are related to the total energy. For instance, the equilibrium lattice constant of a crystal is the lattice constant that minimizes the total energy. If the total energy is calculated, any physical property related to the total energy can be determined.

For Sb_2Te_3 and Bi_2Te_3, structures which are rhombohedral are considered. The equilibrium lattice parameters, the bulk modulus, and its pressure derivative have been computed minimizing the crystal's total energy calculated for the different values of lattice constant

Table 1
The calculated equilibrium lattice parameters (a and c), bulk modulus (B), and the pressure derivative of bulk modulus (B'), together with the theoretical and previous experimental values for Sb_2Te_3 and Bi_2Te_3

Material	Reference	a (Å)	c (Å)	B(GPa)	B'(GPa)
Sb_2Te_3	Present (LDA-SIESTA)	4.256	30.397	64.03	4.94
	Theory (GGA-FLEUR)[a]	4.440	30.290		
	Experimental[b]	4.250	30.350		
Bi_2Te_3	Present (LDA-SIESTA)	4.383	30.487	46.05	4.56
	Theory (GGA-FLUER)[a]	4.530	30.630		
	Experimental[b]	4.383	30.487		

[a]Reference [14].
[b]Reference [25].

by means of Murnaghan's equation of states (eos) [24], and the results are shown in Table 1 along with the experimental and theoretical values. The lattice constants for Sb_2Te_3 and Bi_2Te_3 compounds are found to be a = 4.256 Å, b = 30.397 Å and a = 4.383 Å, b = 30.487 Å, respectively. The lattice parameters obtained are in a good agreement with the experimental and theoretical values [25, 14]. In all our calculations, we have used the computed lattice constants. In the present case, the calculated bulk moduli for Sb_2Te_3 and Bi_2Te_3 are 64.03 and 46.05 GPa, respectively. Unfortunately, there are no theoretical and experimental results for comparing with calculated bulk modulus.

3.2. Electronic Properties

3.2.1. Density of States and Band Structure. For a better understanding of the electronic and optical properties of Sb_2Te_3 and Bi_2Te_3, the investigation of the electronic band structure would be useful. The electronic band structures of rhombohedral Sb_2Te_3 and Bi_2Te_3 single crystals have been calculated along high symmetry directions in the first Brillouin zone (BZ) using the results of SIESTA calculations. The band structures were calculated along the special lines connecting the high-symmetry points Γ(0,0,0), Z (Π,Π,Π), F (Π,Π,0), L (Π,0,0) for Sb_2Te_3 and Bi_2Te_3 in the k-space. The results of the calculation are shown in Fig. 1 for these single crystals.

The energy band structures calculated using LDA for Sb_2Te_3 and Bi_2Te_3 are shown in Fig. 1. As can be seen in Fig. 1, the Sb_2Te_3 and Bi_2Te_3 compounds have an direct band gap semiconductor with the values 0.093 eV and 0.099 eV, respectively. The top of the valance band and the bottom of the conduction band for both compounds positioned at the Γ point of BZ. In conclusion, our band gap values obtained are good agreement with theoretical values and the band gaps have same character with given in Ref. [6, 7]. Band structures of Sb_2Te_3 and Bi_2Te_3 single crystals are compared, band structures of these crystals are highly resemble one another. Thus, on formation of the band structures of Sb_2Te_3 and Bi_2Te_3 the 5s 5p orbitals of Te atoms are more dominant than 5s 5p and 6s 6p orbitals of Sb and Bi atoms. Bi2Te3 and Sb2Te3 also have the particular properties in which the surface states located around the Γ point; both conduction band minimum and valence band maximum of bulk states are located around Γ point, too. In other words, for the low energy range, the surface states and bulk states were not separated in the momentum space (see Fig. 2). From

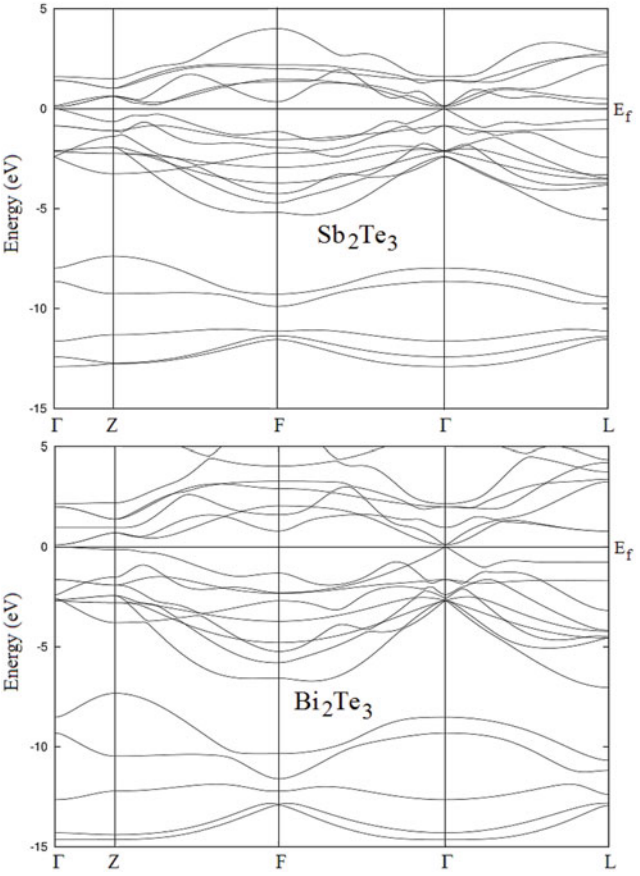

Figure 1. Energy band structure for Sb_2Te_3 and Bi_2Te_3 (Color figure available online).

our data one clearly see that Dirac cone that intersects at the Fermi level at 0.09 Π/a which agrees well with other results [7, 9].

The total and partial densities of states of Sb_2Te_3 and Bi_2Te_3 are illustrated in Fig. 3. As you can see, from this figure, the lowest valence bands occur between about -14 and -12 eV are dominated by Sb 5s and Bi 6s states while valence bands occur between about -12 and -10 eV are dominated by Te 5s states. The highest occupied valance bands are essentially dominated by Te 5p states. The 5p (6p) states of Sb (Bi) atoms are also contributing to the valance bands, but the values of densities of these states are so small compared to Te 5p states. The lowest unoccupied conduction bands just above Fermi energy level are dominated by Sb 5p and Bi 6p states. The 5p states of Te atoms are also contributing to the conduction bands, but the values of densities of these states are so small compared to Sb 5p and Bi 6p states.

3.2.2. Charge Density. The three-dimensional valance charge density distribution of Sb_2Te_3 and Bi_2Te_3 compounds in the plane containing Sb-Te and Bi-Te bonds is illustrated in Fig. 4 and Fig. 5. Examination of the nature of chemical bonding, especially the distribution of valance charges between atoms, is necessary to explain the overall shape.

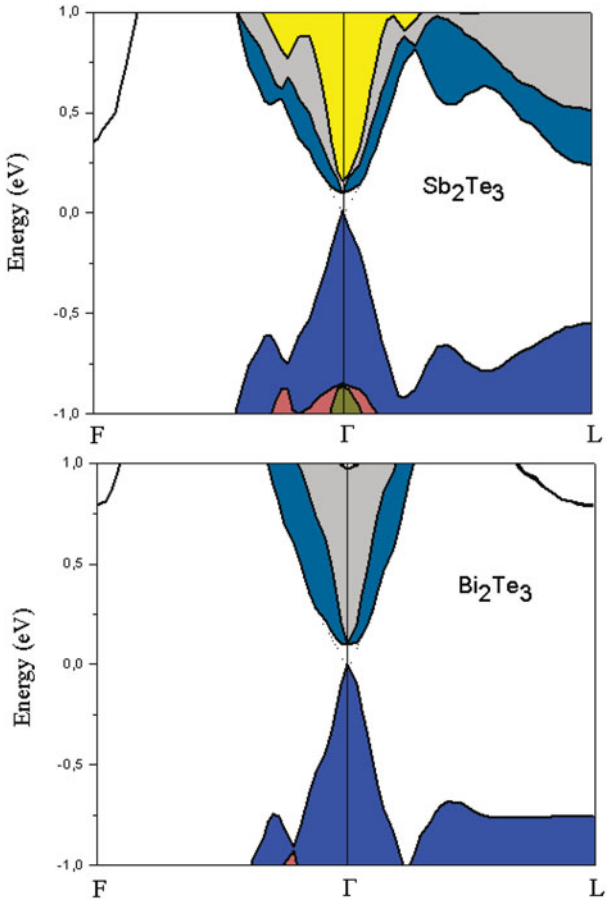

Figure 2. Schematic band structure of the Sb_2Te_3 and Bi_2Te_3 near Γ point of the first Brillouin zone (BZ) (Color figure available online).

The overall shape of the charge distributions suggests covalent bonding of Sb-Te and Bi-Te. Ionicity is directly associated with the character of the chemical bond. It provides us a mean for explaining and classifying the properties of V-VI compounds. The ionicity character is dependent on the total valance charge density by calculating the charge distribution. We have used an empirical formula [26] to obtain an estimated value of the ionicity factor for Sb_2Te_3 and Bi_2Te_3 compounds. In this approach the ionicity parameter is defined as

$$f_i = \frac{1}{2}\left(1 - \cos\left(\frac{E_{AS}}{E_{VB}}\right)\right)$$

Where E_{AS} is the anti-symmetry gap between the two lowest valance bands and the E_{VB} the total valance band width. The calculated value of the ionicity factor for Sb_2Te_3 is 0.089 for $E_{AS} = 1.173\ eV$ and $E_{VB} = 13.192\ eV$, whereas The calculated value of the ionicity factor for Bi_2Te_3 is 0.089 for $E_{AS} = 0.631\ eV$ and $E_{VB} = 14.643\ eV$.

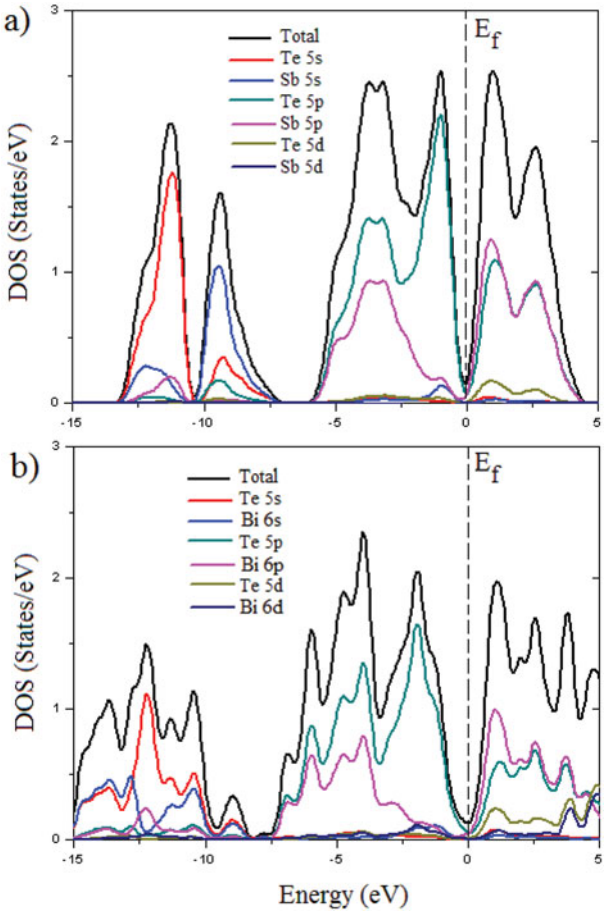

Figure 3. The total (DOS) and projected density of states for (a) Sb_2Te_3 and (b)Bi_2Te_3.

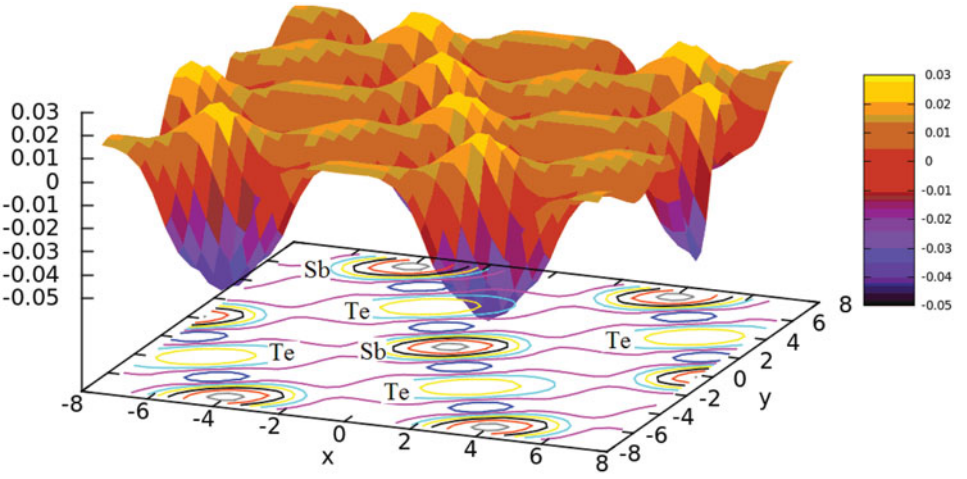

Figure 4. Charge density distribution of the valance charge of Sb_2Te_3.

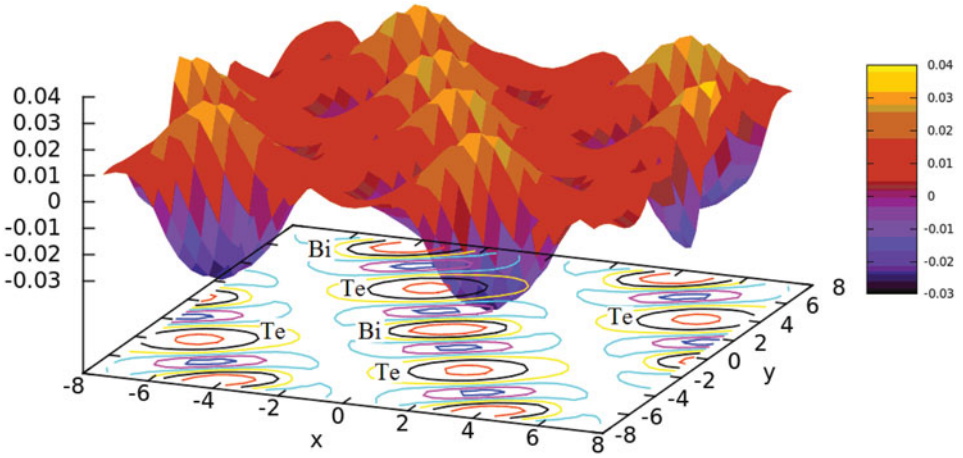

Figure 5. Charge density distribution of the valance charge of Bi_2Te_3.

3.3. Optical Properties

It is well known that the effect of the electric field vector, $\mathbf{E}(\omega)$, of the incoming light is to polarize the material. At the level of linear response, this polarization can be calculated using the following relation [27]:

$$P^i(\omega) = \chi_{ij}^{(1)}(-\omega, \omega).E^j(\omega), \tag{1}$$

where $\chi_{ij}^{(1)}$ is the linear optical susceptibility tensor and it is given by [28]

$$\chi_{ij}^{(1)}(-\omega, \omega) = \frac{e^2}{\hbar\Omega}\sum_{nm\vec{k}} f_{nm}(\vec{k})\frac{r_{nm}^i(\vec{k})r_{mn}^i(\vec{k})}{\omega_{mn}(\vec{k}) - \omega} = \frac{\varepsilon_{ij}(\omega) - \delta_{ij}}{4\pi} \tag{2}$$

where n, m denote energy bands, $f_{mn}(\vec{k}) \equiv f_m(\vec{k}) - f_n(\vec{k})$ is the Fermi occupation factor, Ω is the normalization volume. $\omega_{mn}(\vec{k}) \equiv \omega_m(\vec{k}) - \omega(\vec{k})$ are the frequency differences, $\hbar\omega_n(\vec{k})$ is the energy of band n at wave vector **k.** The $\vec{r}_{nm}$ are the matrix elements of the position operator [28].

As can be seen from Eq. (2), the dielectric function $\varepsilon_{ij}(\omega) = 1 + 4\pi\chi_{ij}^{(1)}(-\omega, \omega)$and the imaginary part of $\varepsilon_{ij}(\omega)$, $\varepsilon_2^{ij}(\omega)$, is given by

$$\varepsilon_2^{ij}(w) = \frac{e^2}{\hbar\pi}\sum_{nm}\int d\vec{k}\, f_{nm}(\vec{k})\frac{v_{nm}^i(\vec{k})v_{nm}^j(\vec{k})}{\omega_{mn}^2}\delta(\omega - \omega_{mn}(\vec{k})). \tag{3}$$

The real part of $\varepsilon_{ij}(\omega)$, $\varepsilon_1^{ij}(\omega)$, can be obtained by using the Kramers-Kroning transformation [28]. Because the Kohn-Sham equations determine the ground state properties, the unoccupied conduction bands as calculated have no physical significance. If they are used as single-particle states in a calculation of optical properties for semiconductors, a band gap problem comes into included in calculations of response. In order to take into account self-energy effects, in the present work, we used the 'scissors approximation' [27].

The known sum rules [29] can be used to determine some quantitative parameters, particularly the effective number of the valence electrons per unit cell N_{eff}, as well as the

effective optical dielectric constant ε_{eff}, which make a contribution to the optical constants of a crystal at the energy E_0. One can obtain an estimate of the distribution of oscillator strengths for both intraband and interband transitions by computing the $N_{eff}(E_0)$ defined according to

$$N_{eff}(E) = \frac{2m\varepsilon_0}{\pi\hbar^2 e^2 Na} \int_0^\infty \varepsilon_2(E) E dE, \tag{4}$$

Where N_a is the density of atoms in a crystal, e and m are the charge and mass of the electron, respectively and $N_{eff}(E_0)$ is the effective number of electrons contributing to optical transitions below an energy of E_0.

Further information on the role of the core and semi-core bands may be obtained by computing the contribution which the various bands make to the static dielectric constant, ε_0. According to the Kramers-Kronig relations, one has

$$\varepsilon_0(E) - 1 = \frac{2}{\pi} \int_0^\infty \varepsilon_2(E) E^{-1} dE. \tag{5}$$

One can therefore define an 'effective' dielectric constant, which represents a different mean of the interband transitions from that represented by the sum rule, Eq. (5), according to the relation

$$\varepsilon_{eff}(E) - 1 = \frac{2}{\pi} \int_0^{E_0} \varepsilon_2(E) E^{-1} dE. \tag{6}$$

The physical meaning of ε_{eff} is quite clear: ε_{eff} is the effective optical dielectric constant governed by the interband transitions in the energy range from zero to E_0, i.e. by the polarizition of the electron shells.

The Sb_2Te_3 and Bi_2Te_3 single crystals have an rhombohedral structure that is optically a uniaxial system. For this reason, the linear dielectric tensor of the Sb_2Te_3 and Bi_2Te_3 compounds have two independent components that are the diagonal elements of the linear dielectric tensor. We first calculated the real and imaginary parts of the x- and z-components of the frequency-dependent linear dielectric function and these are shown in Fig. 6 and Fig. 7. The ε_1^x behaves mainly as a classical oscillator. It vanishes (from positive to negative) at about 1.27 eV, 6.98 eV, 10.24 eV and 17.32 eV (see Fig. 6), whereas the other function ε_1^z is equal to zero at about 1.48 eV, 7.42 eV, 10.42 eV, 17.0 eV, 17.45 eV and 17.50 eV (see Fig. 6) for Sb_2Te_3 compound. The ε_1^x is equal to zero at about 1.89 eV, 6.55 eV, 7.63 eV and 17.41 eV (see Fig. 7), whereas the other function ε_1^z is equal to zero at about 2.04 eV, 6.49 eV, 7.87 eV and 17.37 eV (see Fig. 7) for Bi_2Te_3 compound. The peaks of the ε_2^x and ε_2^z correspond to the optical transitions from the valence band to the conduction band and are in agreement with the previous results. The maximum peak values of ε_2^x and ε_2^z for Sb_2Te_3 are around 1.24 eV and 1.46 eV, respectively, whereas the maximum values of ε_2^x and ε_2^z for Bi_2Te_3 are around 1.74 eV and 1.97 eV, respectively. Spectral dependences of dielectric functions show the similar features for both materials because the electronic configurations of Sb ([Kr], $5s^2$ $5p^3$) and Bi([Xe], $6s^2$ $6p^6$) are very close to each other. In general, there are various contributions to the dielectric function, but Fig. 6 and Fig. 7 show only the contribution of the electronic polarizability to the dielectric function. In

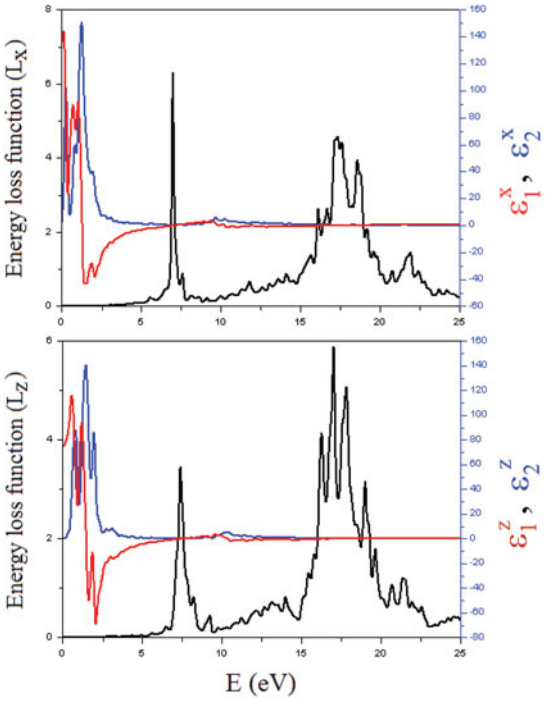

Figure 6. Energy spectra of dielectric function and energy-loss function (L) along the x and z axes for Sb_2Te_3 (Color figure available online).

the range between 0.2 eV and 3 eV, ε_1^z decrease with increasing photon-energy, which is characteristics of an anomalous dispersion. In this energy range, the transitions between occupied and unoccupied states mainly occur between Te 5p states which can be seen in the DOS displayed in Fig. 3. Furthermore as can be seen from Fig. 6 and Fig. 7, the photon–energy range up to 0.1 eV is characterized by high transparency, no absorption and a small reflectivity. The 0.1–3.0 eV photon energy range is characterized by strong absorption and appreciable reflectivity. The absorption band extending beyond 7 eV up to 10 eV is associated with the transitions from the low-lying valance subband to conduction band. Second, we see that above 8 eV, corresponding to the Sb 5s (Bi 6s) and Te 5p. Also, we remark that the region above 10 eV cannot be interpreted in term of classical oscillators. Above 10 eV ε_1 and ε_2 are dominated by linear features, increasing for ε_1 and decreasing for ε_2.

The corresponding energy-loss functions, $L(\omega)$, are also presented in Fig. 6 and Fig. 7. In this figure, L_x and L_z correspond to the energy-loss functions along the x- and z-directions. The function $L(\omega)$ describes the energy loss of fast electrons traversing the material. The sharp maxima in the energy-loss function are associated with the existence of plasma oscillations [30]. The curves of L_x and L_z in Fig. 6 and Fig. 7 have a maximum near 17.32 and 17.02 eV for Sb_2Te_3, respectively, and 17.42 and 17.38 eV for Bi_2Te_3, respectively.

The calculated effective number of valence electrons N_{eff} and the effective dielectric constant ε_{eff} are given in Fig. 8 and Fig. 9. The effective optical dielectric constant, ε_{eff}, shown in Fig. 8 and Fig. 9, reaches a saturation value at about 9 eV. The photon-energy

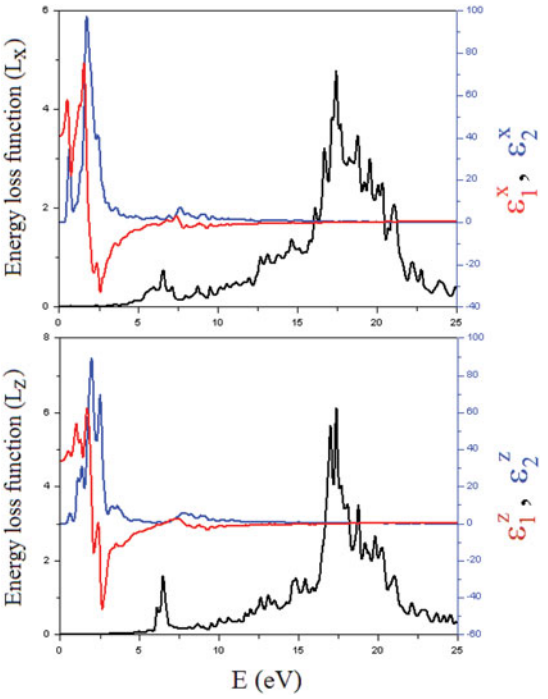

Figure 7. Energy spectra of dielectric function and energy-loss function (L) along the x and z axes for Bi_2Te_3 (Color figure available online).

dependence of ε_{eff} can be separated into two regions. The first is characterized by a rapid rise and it extends up to 4 eV. In the second region the value of ε_{eff} rises more smoothly and slowly and tends to saturations at the energy 9 eV. This means that the greatest contribution to ε_{eff} arises from interband transitions between 0 eV and 4 eV.

As stated above, N_{eff} (determined from the sum rule, eg. eqn (3)) is the effective number of valance electrons per unit cell at the energy $\hbar\omega_0$ (under the condition that the entire interband transitions possible at this frequency ω_0 were made). In the case of Sb_2Te_3 and Bi_2Te_3 the value of N_{eff} increases with increasing photon energy and has tendency to saturate near 9 eV and 20 eV (see Fig. 8 and Fig. 9). Therefore, each of our plots of N_{eff} versus the photon energy for Sb_2Te_3 and Bi_2Te_3 can be arbitrarily divided into two parts. The first is characterized by a rapid growth of N_{eff} up to $\sim$5 eV and extend to 10 eV. The second part shows a smoother and slower growth of N_{eff} and tends to saturate at energies above 30 eV. It is therefore so difficult to choose independent criteria for the estimate of the of valance electrons per unit cell. Recognizing that the two valance sub-bands are separated from each other and are also separated from the low-lying states of the valance band, we can assume a tendency to saturation at energies such that the transition from the corresponding sub-bands are exhausted. In other words, since N_{eff} is determined only by the behavior of ε_2 and is the total oscillator strengths, the sections of the N_{eff} curves with the maximum slope, which correspond to the maxima $dN_{eff}/d\hbar\omega$, can be used to discern the appearance of new absorption mechanism with increasing energy (E = 3.8 eV, 9.5 eV for Sb_2Te_3 and E = 4.2 eV, 9 eV for Bi_2Te_3). The values and behavior of N_{eff} and ε_{eff} for both directions are very close to each other.

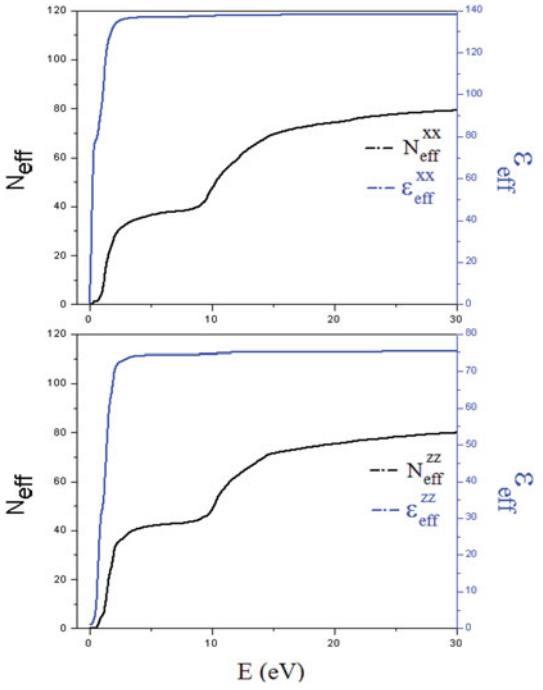

Figure 8. Energy spectra of N_{eff} and ε_{eff} along the x and z axes for Sb_2Te_3.

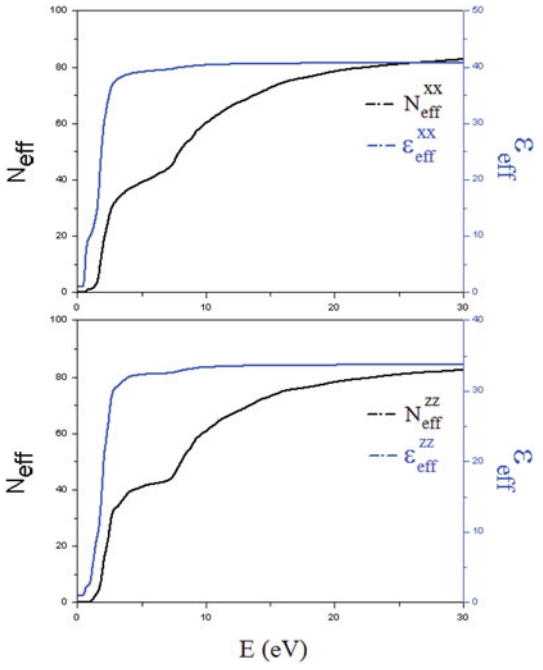

Figure 9. Energy spectra of N_{eff} and ε_{eff} along the x and z axes for Bi_2Te_3.

Conclusion

In the present work, we have made a detailed investigation of the structural, electronic, and frequency-dependent linear optical properties of the Sb_2Te_3 and Bi2Te_3 crystals using the density functional methods. The results of the structural optimization implemented using the LDA are in good agreement with the experimental and theoretical results. We have examined photon-energy dependent dielectric functions, some optical properties such as the energy-loss function, the effective number of valance electrons and the effective optical dielectric constant along the x- and z- axes.

References

1. C. L. Kane and E. J. Mele, Z_2 topological order and the quantum spin hall effect. *Phys Rev Lett*. **95**, 146802.1–146802.4 (2005).
2. B. A. Berneving and S. C. Zhang, Quantum spin hall effect. *Phys Rev Lett*. **96**, 106802.1–106802.4 (2006).
3. J. E. Moore and L. Balents, Topological invariants of time-reversal-invariant band structures. *Phys Rev B*. **75**, 121306.1–121306.4 (2007).
4. C. L. Liang, Kane, and E. J. Mele, Topological insulators in three dimensions. *Phys Rev Lett*. **98**:106803.1–106803.4 (2007).
5. F. Liang and C. L. Kane, Topological insulators with inversion symmetry. *Phys Rev B*. **76**, 045302.1–0.45302.17 (2007).
6. W. Zhang, R. Yu, H. J. Zhang, X. Dai, and Z. Fang: First-principles studies of the three-dimensional strong topological insulator Bi_2Te_3, $Bi_2Se_3$and Sb_2Te_3. *New J Phys*. **12**, 065013.1–165013.14 (2010).
7. H. Zhang, C. H. Liu, X. L. Qi, X. Dai, Z. Fang, and S. C. Zhang: Topological insulators in Bi_2Te_3, Bi_2Se_3 and Sb_2Te_3 with a single Dirac cone on the surface. *Nature Physics*. **5**, 438–442 (2009).
8. L. G. Khvostantsev, A. I. Orlov, N. K. Abrikosov, T. E. Svechnikova, and S. N. Chizhevskaya, Thermoelectric properties and phase transitions in Bi_2Te_3 under hydrostatic pressure up to 9 GPa and temperature up to 300 C. *Phys Stat Sol (a)*. **71**, 49–53 (1982).
9. J. I. Zhang, S. J. Zhang, H. M. Weng, W. Zhang, L. X. Yang, Q. Q. Liu, S. M. Feng, X. C. Wang, R. C. Yu, L. Z. Cao, L. Wang, W. G. Yang, H. Z. Liu, W. Y. Zhao, S. C. Zhang, X. Dai, Z. Fang, and C. Q. Jin, Pressure-induced superconductivity in topological parent compound Bi_2Te_3. *Proc Nat Acad Sci*. **108**, 24–28 (2011).
10. D. D. Frari, S. Diliberto, N. Stein, and J. M. Lecuire: Comparative study of the electrochemical preparation of Bi_2Te, Sb_2Te_3 and $(Bi_xSb_{1-x})_2Te_3$. *Thin Solid Films*. **483**, 44–49 (2005).
11. B. C. Sales, Thermoelectric materials. *Science*. **295**, 1248–1249 (2002).
12. M. J. Huang, R. H. Yen, and A. B. Wang, The influence of the Thomson effect on the performance of a thermoelectric cooler. *Int J Heat Mass Transfer.* **48**, 413–418 (2005).
13. P. P. Dradyumnan and P. P. Swathikrishnan, Thermoelectric properties of Bi_2Te_3 and Sb_2Te_3 and its bilayer thin films. *Indian J Pure and Appl Phys*. **48**, 115–120 (2010).
14. G. Wang and T. Cagin, Electronic structure of the thermoelectric materials Bi_2Te_3 and Sb_2Te_3 from first-principles calculations. *Phys Rev B*. **76**, 075201.1–075201.8 (2007).
15. B. Y. Yavorsky, N. F. Hinsche, I. Mertig, and P. Zahn, Electronic structure and transport anisotropy of Bi_2Te_3 and Sb_2Te_3. *Phys Rev B*. 84:165208.1–165208.7 (2011).
16. J. Choi, S. Choi, J. Choi, Y. Park, H. Y. Park, H. H. Lee, B. C. Woo, and S. Cho, Magnetic properties of Mn-doped Bi_2Te_3 and Sb_2Te_3. phys Stat Sol (b). **241**, 1541–1544 (2004).
17. J. W. Kohn and L. J. Sham: Self-consistent equations including exchange and correlation effects. *Phys Rev.* **140**, A1133–A1138 (1965).
18. D. M. Ceperley and M. J. Adler, Ground state of the electron gas by a stochastic method. *Phys Rev Lett*. **45**, 566–569 (1980).
19. P. Perdew and A. Zunger, Self-interaction correction to density-functional approximations for many-electron systems. *Phys Rev B*. **23**, 5048–5079 (1981).

20. P. Ordejón, E. Artacho, and J. M. Soler, Self-consistent order-N density-functional calculations for very large systems. *Phys Rev B*. **53**, R10441–R10444 (1996).
21. J. M. Soler, E. Artacho, J. D. Gale, A. García, J. Junquera, P. Ordejón, and D. Sánchez-Portal, The SIESTA method for ab initio order-N materials simulation. *J Phys Condens Matt*. **14**, 2745–2779 (2002).
22. O. F. Sankey and D. J. Niklewski, Ab initio multicenter tight-binding model for molecular-dynamics simulations and other applications in covalent systems. *Phys Rev B*. **40**, 3979–3995 (1989).
23. N. Troullier and J. L. Martins, Efficient pseudopotantials foe plane-wave calculations. *Phys Rev B*. **43**, 1993–2006 (1991).
24. F. D. Murnaghan, The compressibility of media under extreme pressures. *Proc Natl Acad Sci U.S.A*. **50**, 244–247 (1944).
25. R. W. G. Wyckoff, *Crystal Structures*. New York: Wiley 1964;**2**:30.
26. K. Unger and H. Newman, The antisymmetric gap and the total width of the valance band of binary compound crystals. *Phys Status Solidi B*. **64**, 117–122 (1974).
27. Z. H. Levine and D. C. Allan, Linear optical response in silicon and germanium including self-energy effects. *Phys Rev Lett*. **63**, 1719–1722 (1989).
28. H. R. Philipp and H. Ehrenreich, Optical properties of semiconductors. *Phys Rev.* **129**, 1550–1560 (1963).
29. O. V. Kovalev, *Representations of the crystallographic space groups. Irreducible representations ınduced representations and corepresentations*. Amsterdam: Gordon and Breach; 1965.
30. L. Marton: Experiments on low-energy electron scattering and energy losess. *Rev Mod Phys*. **28**, 172–183 (1956).